Dielectrophoresis and electrorotation of neurospora slime and murine myeloma cells

Jan Gimsa, Piotr Marszalek, Ulrike Loewe, and Tian Y. Tsong
Department of Biochemistry, University of Minnesota College of Biological Sciences, St. Paul, Minnesota 55108 USA

ABSTRACT Dielectrophoresis and electrorotation are commonly used to measure dielectric properties and membrane electrical parameters of biological cells. We have derived quantitative relationships for several critical points, defined in Fig. A 1, which characterize the dielectrophoretic spectrum and the electrorotational spectrum of a cell, based on the single-shell model (Pauly, H., and H. P. Schwan. 1959. *Z. Naturforsch.* 14b:125–131; Sauer, F. A. 1985. Interactions between Electromagnetic Field and Cells. A. Chiabrera, C. Nicolini, and H. P. Schwan, editors. Plenum Publishing Corp., New York. 181–202). To test these equations and to obtain membrane electrical parameters, a technique which allowed simultaneous measurements of the dielectrophoresis and the electrorotation of single cells in the same chamber, was developed and applied to the study of Neurospora slime and the Myeloma Tib9 cell line. Membrane electrical parameters were determined by the dependence of the first critical frequency of dielectrophoresis (f_{ct1}) and the first characteristic frequency of electrorotation (f_{c1}) on the conductivity of the suspending medium. Membrane conductances of Neurospora slime and Myeloma also were found to be 500 and 380 S m^{-2}, respectively. Several observations indicate that these cells are more complex than that described by the single-shell model. First, the membrane capacities from f_{ct1} (0.81×10^{-2} and 1.55×10^{-2} $F\ m^{-2}$ for neurospora slime and Myeloma, respectively) were at least twice those derived from f_{c1}. Second, the electrorotation spectrum of Myeloma cells deviated from the single-shell like behavior. These discrepancies could be eliminated by adapting a three-shell model (Furhr, G., J. Gimsa, and R. Glaser. 1985. *Stud. Biophys.* 108:149–164). Apparently, there was more than one membrane relaxation process which could influence the lower frequency region of the β-dispersion. f_{ct1} of Myeloma in a medium of given external conductivity were found to be similar for most cells, but for some a dramatically increased f_{ct1} was recorded. Model analysis suggested that a decrease in the cytoplasmatic conductivity due to a drastic ion loss in a cell could cause this increase in f_{ct1}. Model analysis also suggested that the electrorotation spectrum in the counter-field rotation range and f_{c1} would be more sensitive to conductivity changes of the cytoplasmic fluid and to the influence of internal membranes than would f_{ct1}, although the latter would be sensitive to changes in capacitance of the cytoplasmic membranes.

INTRODUCTION

Dielectrophoresis and electrorotation of single biological cells are two closely related phenomena and both can be explained by a unified theory (5, 9, 10, 22, 25, 26). A series of studies on the dielectrophoresis (18, 19, 21, 24, 27) and the electrorotation (1, 2, 6, 8, 14, 16, 20) of cells have proven that both methods are convenient for determining the passive electrical parameters of biological membranes (specific conductivity and capacity). The purpose of this study is to compare the two methods, derive expressions which characterize and relate the dielectrophoresis and the electrorotation spectra of a cell, and use these expressions to determine the dielectric properties of Neurospora slime and Myeloma cells. Two approaches may be used. First, complete dielectrophoretic and electrorotation spectra of cells may be obtained and fit into a single-shell model (8, 14, 20, 21) to determine dielectric properties of the membrane and cytoplasm. Second, certain characteristic points of the dielectrophoresis and the electrorotation of single cells may be measured as functions of experimental parameters (e.g., the external conductivity or cell radius) (1, 19, 21) to determine the dielectric properties. The first approach requires measurements over the frequency range of 1 kHz to 100 MHz for a given field strength which is tedious and time consuming. In the case of dielectrophoresis, an additional problem arises: except for measurements where the dielectrophoretic force is balanced by another counter-acting force (e.g., dielectrophoretic levitation [19]), cell movement must be measured in a chamber which maintains a uniform field gradient and frictional conditions over the whole distance of dielectrophoretic cell movement. This is difficult to achieve. To avoid these technical problems, our experiments focused on measuring the dependence

Address correspondence to Dr. Tsong.
Drs. J. Gimsa and Ulrike Loewe's permanent address is Department of Biology, Humboldt University, Berlin, Germany. Dr. Piotr Marszalek's permanent address is Institute of Electrotechnical Research, Warsaw, Poland.
Piotr Marszalek was a Junior Fullbright Fellow.

of two characteristic points, f_{ct1} and f_{c1}, on the conductivity of the suspending medium. f_{ct1} and f_{c1} are respectively, the first critical frequency for dielectrophoresis and the first characteristic frequency of electrorotation (see Appendix A and Fig. A 1). At f_{ct1}, a cell ceases to move and f_{ct1} is thus less critical to field gradient. For the interpretation of the dielectrophoretic data, an equation describing the dependence of f_{ct1} on the properties of a single-shell object was derived, which corresponds to the well established equation for f_{c1} (2, 10, 13, 16). If the single-shell model is adequate for the description of the dielectrophoretic and electrorotation of cells, electrical parameters of cells determined by the two methods should agree.

MATERIALS AND METHODS

Cells preparations

Murine myeloma cell line Tib9 and Neurospora crassa cells were obtained from American Type Culture Collection (Rockville, MD). These cells were chosen because of their spherical shape in suspension. Myeloma cells were grown in RPMI 1640 medium (Sigma Chemical Co., St. Louis, MO) supplemented with 10% fetal bovine serum, 2% L-glutamine and 0.4% v/v gentamicin (10 mg/ml), at 37°C, in 5% CO_2. For measurements, the cells were collected by centrifugation at 800*g* for 5 min, washed once, under the same conditions, with a 0.3 M sucrose and resuspended in a small amount of 0.3 M sucrose. Myeloma cells were found to be unstable in low ionic strength measuring media. For this reason, cells were transferred into the measuring solution before each measurement and used within 20 min. In all experiments, uniformly spherical cells, having a radius of 5.8 ± 1.2 μm, were chosen.

Neurospora cells were grown according to Fikus et al. (7). Culture flasks were kept in a water bath shaker at 28°C. For experiments, cells from flasks 2 d after inoculation were used. Neurospora cells were prepared like Myeloma except that a 10% sorbitol solution was used instead of 0.3 M sucrose. Experiments on Neurospora were done on cells having a radius of 11 ± 4 μm for dielectrophoresis and of 8.8 ± 1.0 μm for electrorotation measurements, respectively.

The external conductivity was adjusted by addition of the original culture medium to the measuring medium. The conductivity of cell suspensions was monitored by a conductometer (Model 31A, Yellow Springs Instr. Co., Yellow Springs, OH). All experiments were carried out at room temperature, 23 ± 2°C.

Measuring chambers

Dielectrophoretic measurements of Neurospora cells were performed in a chamber made of platinum-plate and a parallel platinum-wire electrode glued to a glass slide. Both electrodes were 15 mm in length and were separated by 0.2 mm. The alternating current (ac) field for this chamber was produced by a generator (model 148A, Wavetek, San Diego, CA) and was monitored by a (model 7704A Tektronix, Beaverton, OR) oscilloscope. A peak-to-peak voltage of 4 V was used. f_{ct1} was determined during sedimentation of cells between the electrode gap by microscopic investigation (21, 27). To measure f_{ct1} of a cell, the generator-frequency was adjusted to the value at which the sedimentation of the cell was not disturbed by the vertically acting dielectrophoretic force (21).

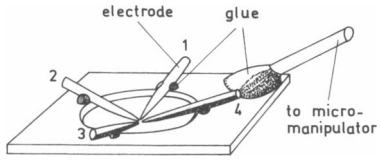

FIGURE 1 Four-electrode chamber used for the electrorotational and dielectrophoretic measurements. The distance between two opposite stainless-needle tips was ~220 μm.

Dielectrophoretic measurements of Myeloma cells and electrorotation measurements of both Myeloma and Neurospora were done in a four-electrode chamber (Fig. 1). The electrodes were made from stainless steel needles glued to a plastic frame. The frame was connected to a three dimensional hydraulic micromanipulator (model MO 203, Narishige USA, Inc., Greenvale, NY) mounted on a three dimensional manipulator (Narishige, model MN-3).

For each measurement, 5 μl of a cell suspension was placed on a microscopic slide. To avoid spreading of the droplet, holes (1.7 mm diam) were punctured in pieces of parafilm "M" (American National Can Co., Greenwich, CT) slightly smaller than the microscopic slides. The parafilm was mounted to the surface by mild heating, forming measuring holes with hydrophobic margins.

Driving signals and field distribution of the four-electrode chamber for electrorotational and dielectrophoretic measurements

Electrorotational measurements: The Transistor–Transistor-Logic (TTL) output (5 V peak-to-peak) of a Wavetek-generator (model 148A) was used to drive a home-made TTL-phase-shifter which produced four 90°-phase shifted TTL-signals. The signal voltage was reduced to a peak-to-peak-voltage of 2.4 V and capacitively coupled to the chamber electrodes. Electrorotational measurements were carried out manually with a stopped watch in the center of the chamber (see reference 15 for field distribution).

Dielectrophoretic measurements: for dielectrophoretic measurements, two 180°-phase-shifted driving signals were used. One signal having a peak-to-peak-voltage of 2.4 V was used only to drive electrode

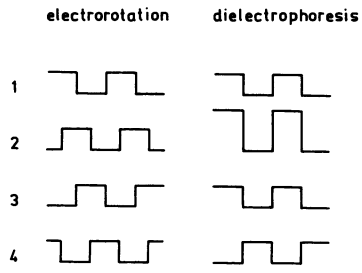

FIGURE 2 Driving signals for the four-electrode chamber shown in Fig. 1.

4 (see Fig. 1); the other signal drove electrodes 1, 2 and 3. To achieve an improved homogeneity of the field for electrode 2, a higher voltage, 4.8 V, was used. A schematic of the driving signals is shown in Fig. 2. Measurements of the first critical frequency were conducted between the center of the chamber and the tip of electrode 4, by adjusting the generator to a frequency at which the lateral movement of single cells ceased. Cells of spherical shape were selected. To minimize the influence of solution streamings on electrorotational and dielectrophoretic measurements, cells were measured in the vicinity of the microscopic slide surface.

THEORETICAL CONSIDERATION

Dielectrophoresis and electrorotation exploit the dynamic effects of ac fields on dielectric objects. These effects of an electric field on the dielectric particle, e.g., a biological cell, suspended in a liquid medium, strongly depend on the relative polarizability of the particle and the medium. In the case of the "ideal" dielectric material, this relative polarizability is determined by the difference between their dielectric permittivities. In the case of lossy dielectric material (like cells suspended in an electrolytic solution), the relative permittivities of the particles as well as the induced dipole moments become complex quantities, depending on the field frequency. It has been shown (10, 13, 22, 25, 27) that the real part of the complex dipole moment, m, of the particle determines the magnitude of the dielectrophoretic force, F_{DP}, experienced by the particle in a nonuniform electric field, while the imaginary part of m determines the torque, T_{ER}, in a rotating field. The corresponding equations are:

$$m = 4\pi\epsilon_0\epsilon_e r^3 EK \quad (1)$$

$$F_{DP} = 2\pi\epsilon_0\epsilon_e r^3 \text{Real}\,(K)\,\nabla E^2 \quad (2)$$

$$T_{ER} = 4\pi\epsilon_0\epsilon_e r^3 \text{Imag}\,(K)\,E^2, \quad (3)$$

where ϵ_0, ϵ_e, r and E stand for the permittivity of the vacuum, the dielectric constant of the suspending medium, the radius of the cell, and the external field strength, respectively. K is the complex frequency dependent part of the induced dipole moment. When Real (m) is positive, the particle is attracted to the stronger electric field and rotates in the same direction as the field rotation. In dielectrophoresis, the particle is attracted to the stronger electric field when F_{DP} is positive and repelled when F_{DP} is negative. In electrorotation, the particle rotates in the same direction as the field rotation when T_{ER} is positive and counter to the field rotation when T_{ER} is negative (see Appendix A). Eq. 3 implies that the electric field is circularly polarized. To find an appropriate expression of K for cells, a certain electrical model must be assumed. This cell model has to be simple enough to permit calculation of the field distribution in the cell and in the surrounding medium. On the other hand, it should reflect the basic electrical properties of the cell which determine its specific polarization processes. In the simplest case, the model consists of a homogeneous conductive sphere (cytoplasm), surrounded by a thin homogeneous shell (cell membrane) having a small conductance. This so called single-shell model, presented in Fig. 3, correctly describes the main polarization processes occurring in the boundaries between the cell membrane and the internal and external media (Maxwell-Wagner polarization [23]). In some cases, dielectric and electrorotational spectra showed deviations from a single-shell spectrum (3, 4, 8, 11, 14, 17). In these cases, a three-shell model (Fig. 3) was proposed to interpret the results (3, 4, 8, 11, 14, 17). The same model was named "double-shell model" by Irimajima et al. (17) and Asami et al. (3, 4) to include the membranes of a cell, namely, the outer and inner membrane. In our view, a two-shell model refers to a cell-wall or glucocalix in addition to the plasma membrane.

The assumption of a second membrane system inside a cell allowed an additional polarization process for the subcellular structures. The internal membrane of the three-shell models was assumed to describe the tonoplast of plant protoplasts (9, 14), the nuclear membrane of lymphocytes (4, 17), the cygote-membrane of oocytes (1, 8) and the inner membrane system of chloroplasts (11) and mitochondria (3). Whether the single- or the three-shell model is appropriate for a certain object depends on its properties as well as on the measuring conditions.

During the dielectrophoresis, the cell experiences no net force at a certain frequency of the external field if the real part of the induced dipole moment is zero. In the low frequency range of the dielectrophoretic spec-

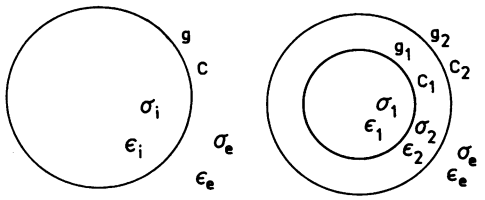

FIGURE 3 Centrally symmetric single-shell model (a) and three-shell model (b) of a cell. Dielectric constants (ϵ) and conductivities (σ) characterize aqueous solutions. Membranes are described by their capacity (C) and specific membrane conductance (g). The subscripts i and e denote internal medium and external medium, respectively. For the three-shell model, the subscript 1 refers to inner membrane and cytoplasmic solution. The subscript 2 refers to outer membrane and the periplasmic solution.

trum, this occurs at f_{ct1}. The reason is that the polarization process of the cell is dominated by charges induced outside the low conducting cell membrane at very low frequencies (causing negative dielectrophoresis). At higher frequencies, this changes to a process mainly characterized by the polarization of the internal solution (causing positive dielectrophoresis). The dispersion mediating this change is characterized by a capacitive bridging of the membrane. Related to this dispersion is a peak of the imaginary part of the induced dipole moment. This peak is characterized by the first characteristic frequency, f_{c1}. If the rotating external field is at this frequency, the cell spins at a maximum speed against the rotation direction of the field (see Appendix A).

To interpret experimental results, the dependence of f_{ct1} and f_{c1} of the single-shell and the three-shell models on model parameters, as defined in Fig. 3, was compared (see Appendices). For single-shell objects, Eq. *A* 6 for f_{ct1} and Eq. *A* 10 for f_{c1} were derived which would allow the internal conductivity, membrane capacity and the membrane conductivity to be determined (see Appendix B). An interesting point is that if the internal conductivity of the cells approaches the external conductivity, both equations predict an opposite behavior for f_{ct1} and f_{c1}, respectively: f_{ct1} increases, whereas f_{c1} decreases. In the case of equal external and internal conductivities, f_{ct1} should reach infinity whereas f_{c1} should reach one third of the value it has when the internal conductivity is much higher than the external conductivity. An experimental test of this property is of special interest because dielectophoretic and electrorotational measurements are usually performed in media of low ionic strengths which may cause ion leakage in cells (12, 17).

For a qualitative explanation of experimental results, dielectrophoretic and electrorotational spectra for the single-shell model (Appendix A), as well as the dependence of f_{ct1} and f_{c1} on the conductivity of the suspending medium for the single- and the three-shell models, were examined (Appendices B and C). Electrorotation spectra for the three-shell model have been analyzed previously (9).

RESULTS AND ANALYSIS

Dielectrophoretic measurements:

Typical distributions of f_{ct1} for Myeloma cell samples at all external conductivities are shown in Fig. 4. Many cells showed similar f_{ct1}-values whereas some had a dramatically increased f_{ct1}. The proportion of cells with very high f_{ct1} was found to increase with time. According to the single-shell model, f_{ct1} would increase when the internal conductivity of cells decreases (Appendix A). To prove that cells had lost their ionic content after 5 to 15

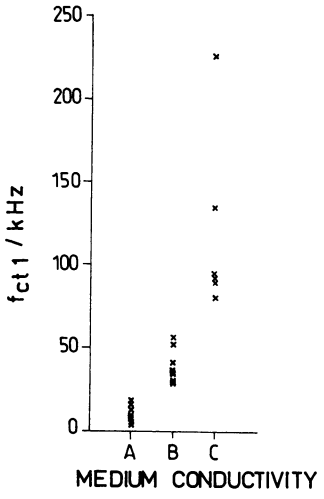

FIGURE 4 Experimentally determined f_{ct1} of single Myeloma cells in media of different conductivities ~15 min after these cells were suspended in the media. *A*, *B*, and *C* correspond to media conductivities of 3.6, 18.3 and 35.5 mS m^{-1}, respectively. Cell radius was 6.0 ± 0.8 μm.

minutes in a low ionic medium, we followed the increase in the conductivity of the suspension after Myeloma cells were transferred to the measuring medium (0.3 M sucrose). For these experiments, cell concentration of about 2%, 100 times the concentration for dielectrophoretic and electrorotational measurements, was used to observe a measurable change of the solution conductivity due to ionic loss of the cells. We found a considerable increase in conductivity, from ~3 mS m^{-1} to >8 mS m^{-1} within 80 min, the latter value being roughly one half that of the Triton X-100 (1 μl Triton per 1 ml cell suspension) lysed cells. For an average cell, having a homogeneous cytoplasm and losing its ions exponentially with time, this increased medium conductivity would correspond to a decrease of the cytoplasmic conductivity from ~300 to 150 mS m^{-1}. Analysis showed that ion leakage consisted of several processes, with three characteristic time constants (<5, 20, and 200 min). Each of the two faster processes contributed ~15% of the total ionic release. We assume that the fastest process was caused by rapid ionic exchanges of surface bound ions and rapid ionic equilibration processes when the cells were transferred from the high ionic washing medium to the low ionic measuring medium. The second process represented the ionic leakage of the cells. The slowest process could result from the lysis of cells, as was observed microscopically, especially for cells suspended in the measuring medium for longer than 30 min.

In the case of Neurospora cells, this behavior was not found in the f_{ct1} measurement. We assume that these

cells were better adapted to the low ionic strength media.

Electrorotation measurements

To find f_{c1} of a cell, the time for one revolution of the cell was determined at 11 different frequencies in logarithmic intervals. For each cell, measurements were started in the high frequency range to prevent ionic leakage due to the rotating field induced transmembrane potential (12). For every frequency the measured rotation speed in radians was normalized to the square of the field strength (2) (see Fig. 5). To find f_{c1} of a cell, Eq. 4 was fit to data using a nonlinear regression program.

$$R = \frac{2R_1 f/f_{c1}}{1 + (f/f_{c1})^2} + \frac{2R_2 f/f_{c2}}{1 + (f/f_{c2})^2} \quad (4)$$

R, f, f_{c1}, f_{c2}, R_1 and R_2 stand for normalized rotation speed, external field frequency, first characteristic frequency, second characteristic frequency, counter-field- and cofield-rotation-peak, respectively (see Fig. A1 *B*). Eq. 4 correctly describes the frequency behavior of a single-shell model (13, 16). Fig. 5 *A* shows two typical experiments using Neurospora slime. The solid curves are the optimized curves for the data points. Both curves were considered good fits. Fig. 5 *B* shows two calculated curves and the data points for Myeloma cells, one of them was considered to be a good fit (4.4 mS m^{-1}) whereas the other was a bad fit (41.1 mS m^{-1}). If a data set could not be fit to Eq. 4, it means the cell deviated from the behavior of the single-shell model.

To judge whether or not a set of data points fit a spectrum predicted by the single-shell model, relative positions of each data point with respect to the fit curve were investigated (14). Almost all spectra of Neurospora cells could be well fit to Eq. 4, whereas Myeloma cells showed systematic deviations. In all cases, where the spectra were considered bad fits, the data points in the counter-field rotation range showed a broader spectrum than that predicted by the single-shell model. The measured rotation speeds of the cell for frequencies close to f_{c1} were lower than the speeds predicted. The measured speeds were always higher than those predicted in the lower and higher frequency ranges of the counter-field rotation (see also reference 20). In the case of Myeloma cells, deviations were insignificant for external conductivities up to 5 mS m^{-1} (Fig. 6). but became severe for external conductivities greater than 10 mS m^{-1}. An exception was found around 22 mS m^{-1} where a large number of well fit spectra were obtained. However, for Neurospora cells, a high percentage of good fit spectra were obtained over the entire conductivity range investigated (Fig. 6).

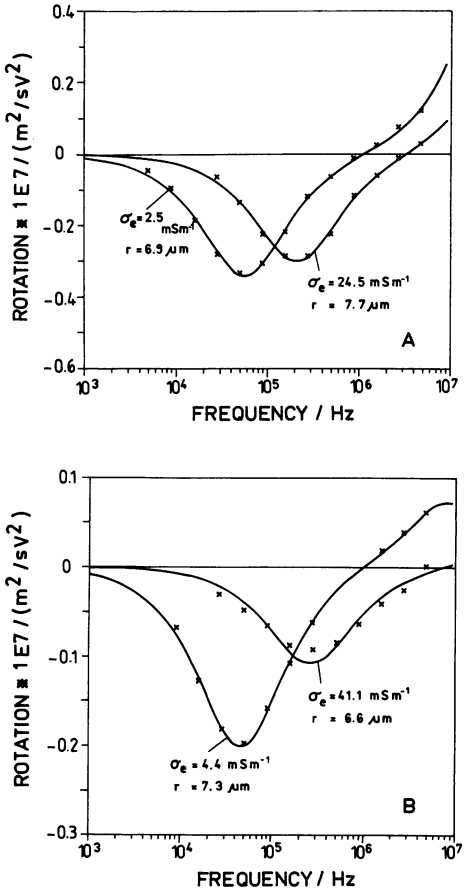

FIGURE 5 Electrorotation spectra of four different cells of Neurospora (*A*) and Myeloma (*B*), at different external conductivities. Solid lines are fit spectra according to Eq. 4.

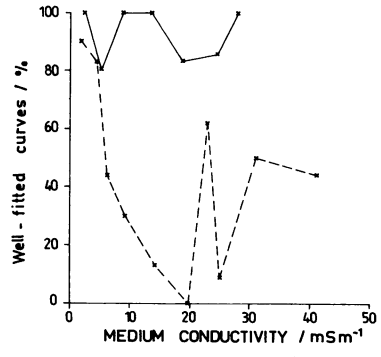

FIGURE 6 Percentages of the electrorotational spectra of Neurospora slime (*solid curve*) and Myeloma cells (*broken curve*) which were considered well fit to Eq. 4, as a function of the external conductivity. Each point was derived from the average of 8 to 13 cell spectra.

Dependence of characteristic frequency on the external conductivity

f_{ct1} and f_{c1} were plotted over the external conductivity for Neurospora and Myeloma cells in Fig. 7. In the case of Neurospora, each data point for f_{ct1} is the mean of all measured cells (7–13 cells). In the case of Myeloma, only lower values of f_{ct1} were used (see Fig. 4). A higher value would indicate the loss of the cytoplasmic ionic content of a cell. Table 1 lists the membrane electrical parameters of Neurospora slime and Myeloma cells obtained by the electrorotation and the dielectrophoresis methods. All values of f_{c1} were obtained by the nonlinear regression fit to Eq. 4. The measurement of f_{c1} was time consuming and a Myeloma cell showed sign of ion leakage during an experiment. Thus, data obtained for Myeloma cells by f_{c1} may not be as reliable as those obtained by f_{ct1}.

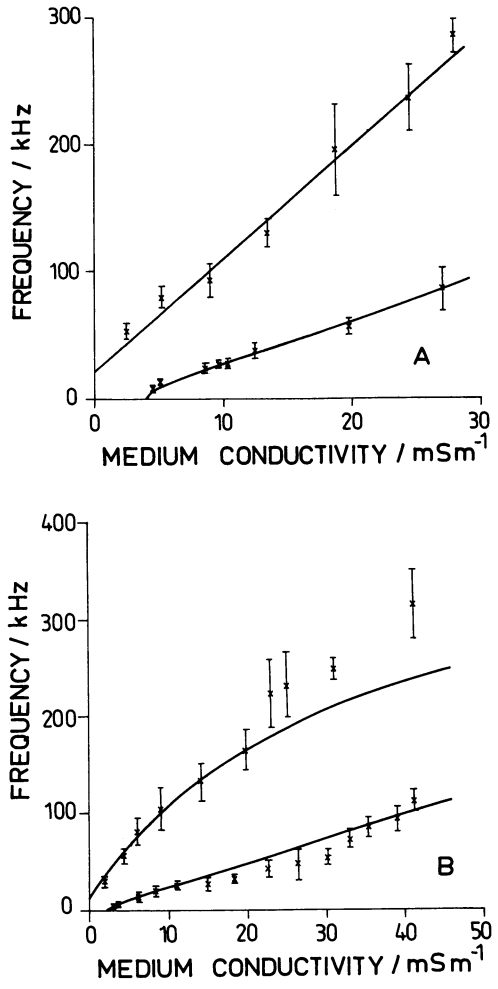

FIGURE 7 f_{ct1} (lower frequency values) and f_{c1} (higher frequency values) of Neurospora slime (A) and Myeloma cells (B) as a function of the external conductivity. The solid lines were optimized curves according to Eq. A6 and Eq. A10 for f_{ct1} and f_{c1}, respectively, using the cell parameters shown in Table 1.

TABLE 1 **Electrical parameters of cells determined by dielectrophoresis and electrorotation**

	Neurospora		Myeloma	
Parameter	f_{ct1}	f_{c1}	f_{ct1}	f_{c1}
Cell radius (μm)	8.8	8.8	5.81	5.81
Membrane capacity ($F\,m^{-2}$)	0.0081	0.0040	0.0155	0.0045
Membrane conductance ($S\,m^{-2}$)	500	500	380	380
Internal conductivity ($S\,m^{-1}$)	0.061	>1.0	>1.0	0.068

The range of values for Neurospora slime was ±10% and for Myeloma was ±20%. Only spectra considered well fit (see text and Fig. 5) were included. For the Myeloma, only data obtained with media conductivities lower than 10 mS m^{-1} were used.

To reduce the deviation of f_{ct1} and f_{c1} measurements for a medium of given external conductivity, every frequency found for a cell was normalized to the average radius of the cell population investigated. Frequencies were multiplied by the actual cell radius and divided by the average radius value of 8.8 μm for Neurospora, and 5.8 μm for Myeloma (2).

DISCUSSION

Influence of the measuring procedure

Suspending cells in the low ionic strength measuring media caused ion leakage which in turn changed the dielectric properties of the cells. This problem was especially acute for the Myeloma cells. However, Fig. 4 indicates that individual cells either retained or lost their cytoplasmic ion contents in a nearly all-or-none manner during the f_{ct1} experiments. Thus, only those cells with higher internal conductivities were selected for analysis (Fig. 7 B). One must also consider ion loss due to the induced transmembrane potentials of the measuring fields. This effect should become more pronounced with decreasing field frequency (4). Ionic leakage would increase membrane conductivity. The measuring fields used in dielectrophoresis and electrorotation experiments are different and should give different effects. In dielectrophoresis, the field lines do not change direction. Only the polarization of the field changes. The areas of the cell membrane under maximal stress are limited to two loci facing the electrode. For electrorotation, this area extends to the ring of membrane laying in the plane of the rotating field. The area of the mem-

brane under stress is much greater in electrorotation than in dielectrophoresis.

The above considerations suggest that the field induced ionic leakage would be higher for a rotating field than for an AC-field. Thus, the f_{c1} experiment would be more influenced by field induced ionic loss. Also, to obtain f_{c1} of a cell, measurements were usually done at 11 different frequencies. So, a cell was exposed to a measuring field for a much longer period of time, and it would experience more stress. An f_{c1} measurement would cause more ion leakage than an f_{ct1} measurement. Interestingly, decreasing internal conductivity would influence the slope of the f_{ct1} and f_{c1} plots over the external conductivity in an opposite sense (Appendix A). It would increase the slope of f_{ct1} but decrease the slope of f_{c1}. Consequently, the calculated membrane capacity for cells which lost their cytoplasmic ions should give an over estimate from the f_{c1} measurement and an under estimate from the f_{ct1} measurement.

Influence of square-topped measuring fields

Except for the dielectrohoretic measurements on Neurospora, square-topped fields having a key-ratio (ratio of field duration and off-time) of 1:1 were used (Fig. 2). The theory, however, was developed for sinusoidal fields. In the case of electrorotation, these fields are theoretically expected to increase the calculated f_{c1} by $< 7\%$ for a single-shell model (13). An analysis on the influence of these fields on f_{ct1} is not yet available.

However, in experiments with Neurospora, we used sinusoidal fields to determine f_{ct1}. The difference between the slopes of the f_{ct1} and f_{c1} plots was much higher than expected for a single-shell model as compared to results obtained with Myeloma. This indicates that the deviations found for both cell species can not be attributed to the influence of the field shape.

Influence of the procedure of f_{c1}-determination

The f_{c1} given for three-shell objects in Appendix C were calculated using the frequency of maximum counter-field rotation. This frequency can not be measured directly. So, we fit a single-shell like curve to the experimental data (see Fig. 5) to determine the frequency of the maximum counter-field rotation. These different procedures may cause some discrepancy between thoeretical and calculated f_{c1} values (Fig. 5 *B*, *curve* for 41.1 mS m^{-1}). However, for the range of model parameters used, the three-shell model yielded counter-field rotation peaks similar in shape to that of a single-shell peak. Nevertheless, the frequencies found could be substantially influenced by the presence of an internal membrane (Appendix C).

Cell electrical parameters

Our attempts to fit f_{ct1} and f_{c1} values obtained with Neurospora slime and Myeloma cells by one set of membrane electrical parameters using Eq. A 6 and Eq. A 10 were unsuccessful. The membrane capacities found from the analysis of the f_{ct1} plots were much higher than those found from the f_{c1} analysis (Table 1 and Fig. 7). This mainly reflects differences in the slopes of the frequency plots from those expected for a single-shell object. Although changes in the cell property can not be ruled out, they can not explain these differences based on our current understanding of the dielectrophoresis and electrorotation phenomena. This indicates that the behavior of neither cell species can be described adequately using the single-shell approach. Irimajiri et al. (17) have reported a similar observation for mouse Lymphoma cells. For Myeloma, the broadening of the electrorotation spectrum (Fig. 5 *B*) provided additional evidence for its deviation from the single-shell model (1, 9, 14). This broadening reduced the number of well-fit spectra (Fig. 6) and caused the f_{ct1} and f_{c1} plots to bend over at higher external conductivity (Fig. 7). The nucleus of a Myeloma cell occupies $\sim 80\%$ of the cytoplasmic volume. Analysis of the three-shell model in Appendix C were done assuming that the internal membrane covers approximately the same volume of the cell. This model could produce a transition in the same external conductivity range for f_{ct1} and f_{c1} (Appendix C). To minimize complication due to the internal membrane like material in Myeloma, we only used f_{ct1} and f_{c1} values obtained for external conductivities lower than 15 mS m^{-1} to calculate the cytoplasmatic membrane properties (see 9 and 20). As can be seen in Fig. 7 *B*, these data gave a good fit to the f_{ct1} and f_{c1} (Eqs. A6 and A10) and the corresponding intercepts at the abscissa and ordinate. For each cell species, the f_{ct1} and f_{c1} values reflect the same membrane conductivity (Table 1). These values are higher than the value of 100 S m^{-2} for mouse Lymphoma cells (17). It must be stated that these values do not necessarily correspond to values found by using dc or ac of very low frequencies because some ionic species that contribute to the ac conductivity do not contribute to the dc conductivity (6).

Our study shows that the single-shell model is not sufficient to describe the f_{ct1} and f_{c1} behaviors of both cell species. The discrepancy between the experimental observation and the behavior of the single-shell model could reflect a slight frequency dependence of membrane capacitance, anisotropy of the cell interior, or the existence of cytoplasmic membrane like material, such

as organelles or a large nucleus. Specific source has not been identified. However, introducing a second membrane relaxation process, using the three-shell model, allows a qualitative explanation of our experimental results. In many cases, the three-shell model showed a steeper increase in f_{c1} with increasing external conductivity (compare curve 4 of Fig. B1*A* with curve 6 of Fig. C1*B*). Curves 1, 2, and 3 given in Fig. C1 show a transition range for f_{ct1} and f_{c1} similar to that found for Myeloma. In other cases, this transition is shifted to experimentally nonaccessible external conductivity values (curves 4 and 5 in Fig. C1). This might be true for Neurospora slime.

APPENDIX A

Properties of the dielectrophoretic and electrorotational spectrum of the single-shell model

The properties of a spherical single-shell model have been examined in the β dispersion range. The frequency-dependent part of the induced dipole moment, K, can be written in the form (10, 16, 25) (see Eq. 1):

$$K = \frac{\omega^2\epsilon_0^2 A_1 + j\omega\epsilon_0 B_1 + C_1}{\omega^2\epsilon_0^2 A_2 + j\omega\epsilon_0 B_2 + C_2}, \qquad \text{(A1)}$$

where $j = \sqrt{-1}$ and $\omega = 2\pi f$. A_1, A_2, B_1, B_2, C_1, and C_2 are quantities which depend on the frequency-independent conductivities and dielectric constants of the three phases shown in Fig. 3, as well as, on the size of the sphere. By introducing area-specific parameters to describe membrane properties and ignoring very small terms, these quantities can be expressed as:

$$\begin{aligned} A_1 &= \epsilon_e\epsilon_i/r + C(\epsilon_e - \epsilon_i)/\epsilon_0 \\ A_2 &= -2\epsilon_e\epsilon_i/r - C(2\epsilon_e + \epsilon_i)/\epsilon_0 \\ B_1 &= C(\sigma_i - \sigma_e)/\epsilon_0 \\ B_2 &= C(\sigma_i + 2\sigma_e)/\epsilon_0 \\ C_1 &= g(\sigma_i - \sigma_e) - \sigma_i\sigma_e/r \\ C_2 &= g(\sigma_i + 2\sigma_e) + 2\sigma_i\sigma_e/r, \end{aligned} \qquad \text{(A2)}$$

where r, C, g, ϵ_e, ϵ_i, σ_e, σ_i, and ϵ_0 stand for cell radius, membrane capacity, area specific membrane conductivity, external and internal dielectric constant, external and internal conductivity and permittivity of vacuum, respectively. Dielectrophoretic force and electrorotational torque are proportional to the real and the imaginary parts of the dimensionless parameter K, respectively. Two corresponding dielectrophoretic and electrorotational spectra are shown in Fig. A1.

There are five points characteristic for each spectrum (Fig. A1). For a dielectrophoretic spectrum they are: three different plateaus for the force (F_1, F_2, and F_3) acting on the particle in different frequency ranges and the two critical frequencies (f_{ct1}, f_{ct2}). At these frequencies the dielectrophoretic force ceases to exist. The two changes of the dielectrophoretic force from F_1 to F_2 and from F_2 to F_3 can be attributed to the dispersion of the membrane polarization and the dispersion of the cytoplasm polarization caused by conductivity effects,

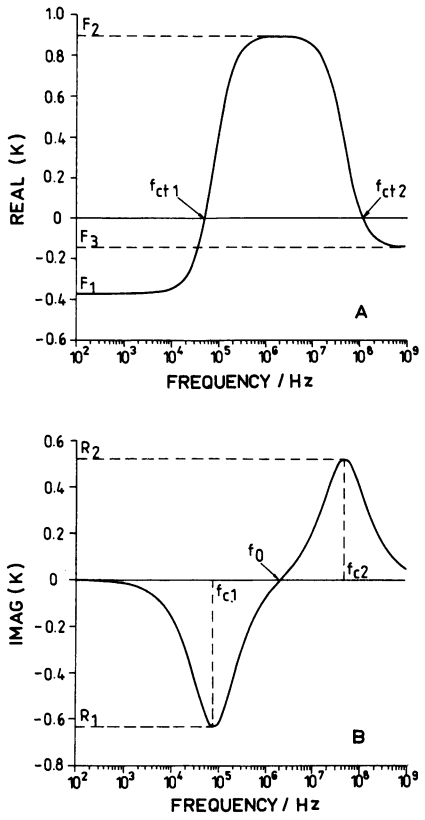

FIGURE A1 Typical dielectrophoretic (*A*) and electrorotational (*B*) spectra of a single-shell model. Five characteristic points of each spectrum are defined.

respectively. In the electrorotational spectrum these dispersions are expressed as rotation peaks at two characteristic frequencies, f_{c1} and f_{c2}. At these characteristic frequencies the rotation speed of the cell against or along the field rotation reaches a maximum, R_1 and R_2, respectively. At f_0, the rotation ceases. To further evaluate the influence of membrane parameters, we have derived approximate equation for each of the 10 points. Valuable information about all properties of the cell-model can be obtained using these approximations. The five points for the dielectrophoretic spectrum are:

$$F_1 = \frac{rg(\sigma_i - \sigma_e) - \sigma_i\sigma_e}{rg(\sigma_i + 2\sigma_e) + 2\sigma_i\sigma_e} \qquad \text{(A3)}$$

$$F_2 = \frac{\sigma_i - \sigma_e}{\sigma_i + 2\sigma_e} \qquad \text{(A4)}$$

$$F_3 = \frac{\epsilon_i - \epsilon_e}{\epsilon_i + 2\epsilon_e} \qquad \text{(A5)}$$

$$f_{ct1} = \frac{1}{2\pi rC}\sqrt{\frac{2\sigma_i\sigma_e - rg(\sigma_i - 4\sigma_e)}{(\sigma_i + 2\sigma_e)(1/\sigma_e - 1/\sigma_i)} - g^2r^2} \qquad \text{(A6)}$$

$$f_{ct2} = \frac{1}{2\pi\epsilon_0}\sqrt{\frac{(\sigma_i - \sigma_e)(\sigma_i + 2\sigma_e)}{(\epsilon_e - \epsilon_i)(\epsilon_i + 2\epsilon_e)}}. \qquad \text{(A7)}$$

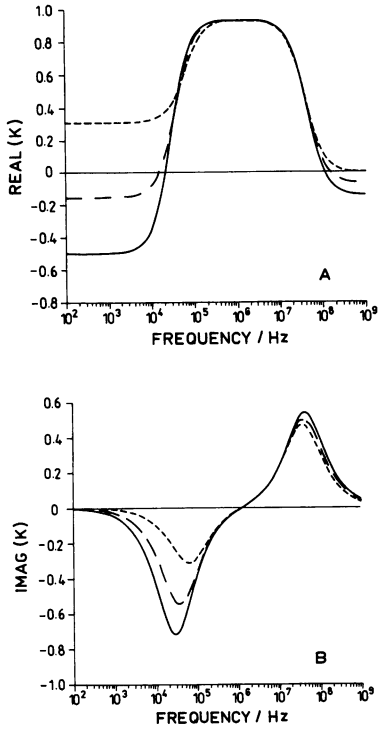

FIGURE A2 Effects of membrane conductivity, g, and internal dielectric constant, ϵ_i, on the shape of dielectrophoretic (A) and electrorotational (B) spectra. Parameters used were: solid lines (g = 0; ϵ_i = 50), broken lines (g = 500 S m^{-2}; ϵ_i = 60), dashed lines (g = 2000 S m^{-2}; ϵ_i = 80).

The five points for the electrorotational spectrum are:

$$R_1 = \frac{-1.5\sigma_i}{(\sigma_i + 2\sigma_e)\,[gr(1/\sigma_e + 2/\sigma_i) + 2]} \tag{A8}$$

$$R_2 = \frac{1}{2}\left(\frac{\epsilon_e - \epsilon_i}{\epsilon_i + 2\epsilon_e} + \frac{\sigma_i - \sigma_e}{\sigma_i + 2\sigma_e}\right) \tag{A9}$$

$$f_{c1} = \frac{1}{2\pi rC}\left(\frac{1}{1/2\sigma_e + 1/\sigma_i} + rg\right) \tag{A10}$$

$$f_{c2} = (\sigma_i + 2\sigma_e)/[2\pi\epsilon_0(\epsilon_i + 2\epsilon_e)] \tag{A11}$$

$$f_0 = 1/2\pi\sqrt{\sigma_i/[\epsilon_0 rC(\epsilon_e/\sigma_e - 2\epsilon_i/3\sigma_i)]}\,. \tag{A12}$$

Derivations of Eqs. A3–A12 assumed that the membrane thickness is very small compared to the cell radius, that the internal conductivity never decreased below the external conductivity, and that the membrane conductivity was at least two orders of magnitude lower than the external conductivity.

To test the reliability of these approximations, values derived from these equations were compared with those calculated from the complete model by the computer. The errors due to these approximations was typically <5%, except for very high membrane conductivities (>1,000 S m^{-2}). In such cases, the errors can reach 20% for F_2, R_1 and f_0. Eqs. A3, A6, and A7 for F 1, f_{ct1} and f_{ct2}, respectively, were precise, with errors smaller than 2.5%. The close relationship between the dielectrophoretic and the electrorotational spectra of a particle can be demonstrated by the Cole–Cole-plots of K (9). In these plots, the following relationships can be demonstrated graphically: the peak values of the imaginary part of K depend on the strength of the related dispersion: $R_1 = (F_1 - F_2)/2$ and $R_2 = (F_2 - F_3)/2$. The characteristic frequencies of electrorotation are identical to the frequencies of the steepest slopes in the dielectrophoretic plots.

To examine how different parameters might influence a spectrum, we considered a model cell with a radius of 6 μm. The following sets of parameters were chosen: cytoplasmic conductivity 0.5 S m^{-1} and dielectric constant 50; external conductivity 5.0 mS m^{-1} and dielectric constant 80; membrane area specific conductivity 1.0 S m^{-2} and capacity 8.9 × 10^{-3} F m^{-2}. Calculations were based on the complete model (16, 25), in which the cell membrane is treated as a homogeneous phase. A membrane thickness of 8 nm was used to recalculate the area specific parameters (13, 16). We obtained a membrane conductivity of 8 × 10^{-9} S m^{-1}, which corresponded to an area specific conductivity of 1 S m^{-2}, and a membrane dielectric constant of 8, which corresponded to membrane capacitance of 8.9 × 10^{-3} F m^{-2}. Fig. A2 shows the calculated dielectrophoresis and electrorotation spectra using three sets of values for membrane conductivity and interior dielectric constant. We will limit our discussion to dielectrophoresis spectra, because electrorotation spectra have been discussed in details elsewhere (9, 10, 16, 25).

From Fig. A2, it can be seen that when membrane conductivity was zero, the normalized force F_1 reached −0.5 (*curve with solid line*).

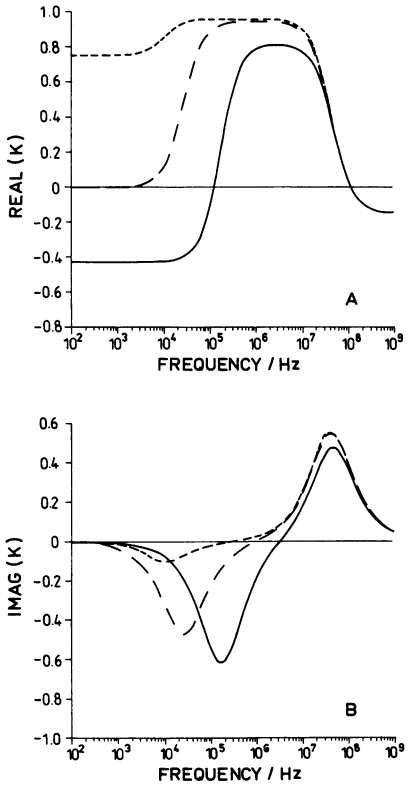

FIGURE A3 Effects of external conductivity, σ_e, on the dielectrophoretic (A) and electrorotational (B) spectra. The membrane conductivity was 500 S m^{-2}. σ_e was 30 mS m^{-1} for the solid lines, 3 mS m^{-1} for the broken lines, and 0.3 mS m^{-1} for the dashed lines.

Under the additional assumption that the internal conductivity was much higher than that of the external medium, F_2 would reach 1. This would be related to a counter-field rotation peak of $R_1 = -0.75$. If the membrane conductivity reached a value greater than $\sigma_i\sigma_e/[r(\sigma_i - \sigma_e)]$, the low frequency part of the spectrum would no longer be negative (see Eq. A3). The high frequency part of the dielectrophoretic spectrum is determined by the dielectric constants of cytoplasm and external medium. If they are equal, the dielectrophoretical force disappears (*curve with dashed line*).

Fig. A3 shows effects of external medium conductivity changes on the spectra. For a given membrane conductivity, the negative part of the dielectrophoretic spectrum disappears at a certain external conductivity. This conductivity can be determined experimentally. If the conductivity is much higher for the internal than for the external media, the membrane conductivity can be estimated with $g = \sigma_e/r$ (see Eq. A3).

APPENDIX B

Dependence of f_{ct1} and f_{c1} on external conductivity for a single-shell model

f_{ct1} and f_{c1} can be easily measured experimentally. We examined how f_{ct1} and f_{c1} would depend on cell electrical parameters by varying the external conductivity up to the experimentally available value of 50 mS m^{-1}. A cell radius of 6 μm was assumed.

Fig. B1 *A* shows that f_{ct1} was linearly dependent on the external conductivity when the membrane conductivity was low and the internal conductivity was at least three times greater than the highest external conductivity (*curves* 1 and 5). The slope of these straight lines reflects the membrane capacity (5, 19, 21) (compare *curves* 1 and 5). Under the above assumptions, Eq. A6 becomes:

$$f_{ct1} = \sigma_e/(\sqrt{2}\pi rC). \qquad \text{(B1)}$$

This indicates that the slope of an f_{ct1} plot is $\sqrt{2}$ times smaller than that of a f_{c1} plot under the same conditions (see Eq. A10). When the membrane conductivity is high, f_{ct1} can not be measured in a medium of low external conductivity because there will be no negative dielectrophoresis in this case (see Fig. A2 *A* and A2 *B*). This corresponds to a negative expression under the square root of Eq. A6. In the case of low internal conductivities, f_{ct1} increased dramatically when the external conductivity approached the internal conductivity (either by increasing the external or decreasing the internal conductivity). To find significant differences in f_{ct1} due to a decreased internal conductivity, the latter had to be reduced to less than one half the value of the corresponding external conductivity. f_{ct1} doubled if the internal conductivity dropped below 110% of the external conductivity. However, this increase was related to a decrease of the dielectrophoretic force (see Eq. A4). Note that in contradiction to the behavior of f_{ct1}, f_{c1} decreases if the internal conductivity drops. For low values of the membrane conductivity (<1 S m^{-2}), f_{ct1} plots started close to 0 kHz (*curves* 1, 3 and 5). For higher membrane conductivities, a steep increase of f_{c1} to a certain value of extremely low external conductivities was seen (<1 mS m^{-1}) (*curves* 2 and 4). Experimentally, it would be difficult to achieve an external conductivity of less than 1 mS m^{-1}. This steep increase is not predicted by Eq. A10. For higher external conductivities (>1 mS m^{-1}), curves for high and low membrane conductivities were parallel if other parameters were equal (*curves* 1 and 2, or 3 and 4). f_{c1}-curves for low internal conductivities (0.05 S m^{-1}) already differed from curves with a high internal conductivity (0.5 S m^{-1}) if the external conductivity reached 1/10 (0.005 S m^{-1}) that of the internal conductivity. The f_{ct1} plots showed differences only in the case that the external conductivity reached at least one half the internal conductivity.

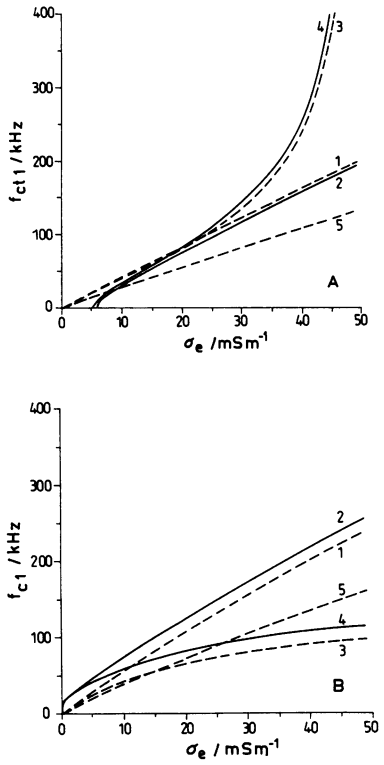

FIGURE B1 Effects of external conductivity on f_{ct1} (*A*) and f_{c1} (*B*) of a single-shell model. The internal and external dielectric constants were 50 and 80, respectively. Membrane conductivities were 1 S m^{-2} and 1,000 S m^{-2} for the dashed and solid lines, respectively. The internal conductivities were 0.05 S m^{-1} (*curves* 3 and 4) and 0.5 S m^{-1} (*curves* 1, 2 and 5). Except for *curve* 5 (1.33×10^{-2} *F* m^{-2}), the membrane capacity was 0.89×10^{-2} *F* m^{-2}.

This suggests that f_{c1} is more sensitive to the properties of the cell interior than f_{ct1} is, whereas f_{ct1} is more useful for determining the membrane capacity. For electrorotation, the membrane conductivity can be deduced by extrapolating f_{c1} to an external conductivity of 0, assuming that for every low external conductivities the internal conductivity is much higher. This yields the membrane conductivity, $g = 2\pi f_{c1}C$ (see Eq. A10). For dielectrophoresis the membrane conductivity can be determined from the point where the negative dielectrophoresis disappears. In this case the membrane conductivity becomes $g = \sigma_e/r$ (see Eq. A3). A disadvantage for measuring this point is that at external conductivities close to it, the negative dielectrophoretical force decreases abruptly so that the frequency measurement becomes less precise. This is not the case for electrorotation.

APPENDIX C

Dependence of f_{ct1} and f_{c1} on external conductivity for a three-shell model

The same cell radius (6 μm) would be used in our analysis of the threeshell model. The spherical internal membrane system was as-

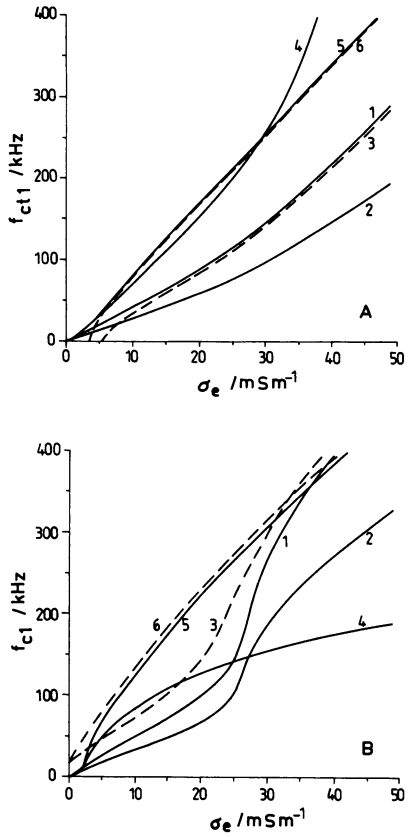

FIGURE C1 f_{ct1} (A) and f_{c1} (B) for a three-shell model. Except for *curve* 2 (1.33×10^{-2} F m^{-2}), membrane capacitances for both outer- and inner-membranes were 0.89×10^{-2} F m^{-2} for all curves. The dielectric constant of the internal medium was 50 and of the external medium was 80. Other parameters used in the calculation are listed in Table 2.

sumed to cover about 80% of the cell volume having a radius of 5.5 μm (see Fig. 3). Similar to the one-shell model, the complete model (9, 25) would be considered assuming a certain membrane dielectric constant and conductivity for a membrane thickness of 8 nm. These values were recalculated into area specific parameters. For a better understanding of the behavior of f_{ct1} and f_{c1}, calculations for five parameter-combinations are shown in Fig. C1.

These curves show that the behavior of the three-shell model is qualitatively different from that of the single-shell object. Some of them (*curves* 1, 2 and 3) showed a clear transition in the f_{c1} plots, expressed by a steep f_{c1} increase followed by a change of the slope. A slope change could be found in f_{ct1} plots in the same external conductivity range. Nevertheless, the transition was not as obvious. Comparisons with the one-shell model using the same parameters for the external membrane system showed that in most cases the plots for f_{ct1} and f_{c1} were similar or identical at very low external conductivities (<2.5 mS m^{-1}). In other cases (f_{c1} *curve* 6 and f_{ct1} *curves* 3, 4, 5 and 6), only the starting values and values for an external conductivity smaller than 0.2 m S^{-1} were identical. These results show that the assumption of a wrong cell model can lead to wrong membrane parameters. It was found that the plots of f_{ct1} and f_{c1} did not always showed clear deviations from a single-shell behavior. The reasons for this may be: (*a*) a transition may have already occurred at experimentally inaccessible external conductivities; (*b*) the deviations of the measured points are too big to show the transition (see *curve* 3); (*c*) there might be more than two membrane relaxations involved. This would probably lead to a smoother transition. However, in every case, by examining the measured cell spectra for their deviations from a single shell-like shape and by the comparison of f_{ct1} and f_{c1} plots for their consistency, new information would be forthcoming for deriving cell parameters.

TABLE 2 Parameters used for the simulation in Fig. C1

Cruve	Conductivities in $S\,m^{-1}$: Inner sphere	Conductivities in $S\,m^{-1}$: Intermembraneous space	Membrane conductivities in $S\,m^{-2}$: Internal	Membrane conductivities in $S\,m^{-2}$: External
1	0.5	0.5	1	1
2	0.5	0.5	1	1
3	0.5	0.5	1,000	1,000
4	0.05	0.05	1	1
5	0.5	0.05	1	1
6	0.5	0.05	1	1,000

We thank C. J. Gross for help with the manuscript.

This work was supported by a grant from the United States Office of Naval Research.

Received for publication 11 March 1991 and in final form 23 May 1991.

REFERENCES

1. Arnold, W. M., R. K. Schmutzler, S. Al-Hasani, D. Krebs, and U. Zimmermann. 1989. Differences in membrane properties between unfertilized and fertilized single rabbit oocytes demonstrated by electrorotation. Comparison with cells from early embryos. *Biochim. Biophys. Acts.* 979:142–146.
2. Arnold, W. M., and U. Zimmermann. 1982. Rotating-field induced rotation and measurement of the membrane capacitance of single mesophyll cells of *Avena sativa*. *Z. Naturforsch.* 37c:908–915.
3. Asami, K., and A. Irimajiri. 1984. Dielectric analysis of mitochondria isolated from rat liver. II. Intact mitochondria as simulated by a double-shell model. *Biochim. Biophys. Acts.* 778:570–578.
4. Asami, K., Y. Takahashi, and S. Takashima. 1989. Dielectric properties of mouse lymphocytes and erythrocytes. *Biochim. Biophys. Acta.* 1010:49–55.
5. Chizmadzhev, Yu. A., P. I. Kuzmin, and V. Ph. Pastushenko. 1985. Theory of the dielectrophoresis of vesicles and cells. Biol. Membr. 11:1147–1161. (In Russian.)
6. Engel, J., E. Donath, and J. Gimsa. 1988. Electrorotation of red cells after electropoation. *Stud. Biophys.* 125:53–62.
7. Fikus, M., E. Grzesiuk, P. Marszalek, S. Rozycki, and J. J. Zielinski. 1985. Electrofusion of Neurospora crassa slime cells. *FEMS (Fed. Euro. Microbiol. Soc.) Lett.* 27:123–127.
8. Fuhr, G., F. Geissler, T. Mueller, R. Hagedorn, and H. Torner. 1987. Differences in the rotational spectra of mouse oocytes and zygotes. *Biochim. Biophys. Acta.* 930:65–71.
9. Fuhr, G., J. Gimsa, and R. Glaser. 1985. Interpretation of

electrorotation of protoplasts. I. Theoretical considerations. *Stud. Biophys.* 108:149–164.

10. Fuhr, G., R. Glaser, and R. Hagedorn. 1986. Rotation of dielectrics in a rotating high frequency field; model experiments and theoretical explanation of the rotation effect of living cells. *Biophys. J.* 49:395–402.
11. Fuhr, G., P. Roesch, T. Mueller, V. Dressler, and H. Goering. 1990. Dielectric spectroscopy of chloroplasts isolated from higher plants: characterization of the double-membrane system. *Plant Cell Physiol.* 31:975–985.
12. Georgiewa, R., J. Gimsa, U. Loewe, and R. Glaser. 1989. AC-field-induced KCl leakage from human red cells at low ionic strength. *Bioelectrochem. Bioenerg.* 22:255–270.
13. Gimsa, J., E. Donath, and R. Glaser. 1988. Evaluation of data of simple cells by electrorotation using square-topped fields. *Bioelectrochem. Bioenerg.* 19:389–396.
14. Gimsa, J., G. Fuhr, and R. Glaser. 1985. Interpretation of electrorotation of protoplasts. II. Interpretation of experiments. *Stud. Biophys.* 109:5–14.
15. Gimsa, J., R. Glaser, and G. Fuhr. 1988. Remarks on the field distribution in four electrode chambers for electrorotational measurements. *Stud. Biophys.* 125:71–76.
16. Glaser, R., and G. Fuhr. 1986. Electrorotation of single cells—a new method for assessment of membrane properties. *In* Electric Double Layers in Biology. M. Blank, editor. Plenum Publishing Corp., New York. 227–242.
17. Irimajiri, A., Y. Doida, T. Hanai, and A. Inouye. 1978. Passive electrical properties of cultured Murine lymphoblast (L5178Y) with reference to its cytoplasmic membrane, nuclear envelope, and intracellular phases. *J. Membr. Biol.* 38:209–232.
18. Jones, T. B. 1986. Dielectrophoretic force in axisymmetric fields. *J. Electrostat.* 18:55–62.
19. Kaler, K. V. I. S., and T. B. Jones. 1990. Dielectrophoretic spectra of single cells determined by feedback-controlled levitation. *Biophys. J.* 57:173–182.
20. Lovelace, R. V. E., D. G. Stout, and P. I. Steponkus. 1984. Protoplast rotation in a rotating electric field: the influence of cold acclimation. *J. Membr. Biol.* 82:157–166.
21. Marszalek, P., J. J. Zielinski, and M. Fikus. 1989. Experimental verification of a theoretical treatment of the mechanism of dielectrophoresis. *Bioelectrochem. Bioenerg.* 22:289–298.
22. Pastushenko, V. Ph., P. I. Kuzmin, and Yu. A. Chizmadzhev. 1985. Dielectrophoresis and electrorotation: a unified theory of spherically symmetrical cells. *Stud. Biophys.* 110:51–57.
23. Pauly, H., and H. P. Schwan. 1959. The impedance of a suspension of spherical particles surrounded by a shell. *Z. Naturforsch.* 14b:125–131. (In German.)
24. Pohl, H. A. 1978. Dielectrophoresis. Cambridge University Press, London.
25. Sauer, F. A., and R. N. Schloegl. 1985. Torques exerted on cylinders and spheres by external electromagnetic fields: a contribution to the theory of field-induced cell rotation. *In* Interactions Between Electromagnetic Fields and Cells. A. Chiabrera, C. Nicolini, and H. P. Schwan, editors. Plenum Publishing Corp., New York, 203–251.
26. Schwan, H. P. 1989. Dielectrophoresis and rotation of cell. *In* Electroporation and Electrofusion in Cell Biology. E. Neumann, A. E. Sowers, and C. A. Jordan, editors. Plenum Publishing Corp., New York. 3–21.
27. Zielinski, J. J., P. Marszalek, and M. Fikus. 1989. A new method for the investigation of cellular dielectrophoresis. *Z. Naturforschung.* 44c:845–848.